ARTICLE   OPEN

The critical role of dimethylamine in the rapid formation of iodic acid particles in marine areas

An Ning [1], Ling Liu[1], Shaobing Zhang[1], Fangqun Yu[2], Lin Du [3], Maofa Ge [4] and Xiuhui Zhang [1]✉

Marine new particle formation (NPF) can affect cloud condensation nuclei (CCN) in the global atmosphere. Recently, iodic acid (IA) has been identified as a critical driver for marine NPF. However, atmospheric observations of IA cannot be associated with predicted particle formation rates. Given the complexity of atmospheric components, other species may promote IA particle formation. As an efficient stabilizer for acidic precursors, dimethylamine (DMA) has a wide distribution over the oceans. Hence, we investigated the nucleation process of DMA and IA under different atmospheric conditions and uncovered the corresponding nucleating mechanism using a quantum chemical approach and Atmospheric Cluster Dynamics Code (ACDC). The findings show that DMA can structurally stabilize IA via hydrogen and halogen bonds, and the clustering process is energy barrierless. Moreover, DMA can enhance the formation rate of IA clusters by five orders of magnitude, and its efficiency in promoting IA cluster formation is much higher than that of NH_3. Compared to the nucleation via sequential addition of IA, the IA-DMA nucleation plays a more dominant role in nucleation kinetic. Thus, the effect of DMA on enhancing IA cluster stability and formation rate cannot be ignored, especially in the regions near the source of IA and DMA emissions. Broadly, the proposed IA-DMA nucleation mechanism may help to explain some missing sources of particles and, thus intensive marine NPF events.

INTRODUCTION

Marine aerosol acts as the most important natural aerosol system in the world, significantly affecting global radiation balance and climate system through further conversion to cloud condensation nuclei (CCN)[1,2]. New particle formation (NPF) initiated via the nucleating of gaseous molecules provides an important source of atmospheric aerosol[3,4]. Hence, to better understand the marine aerosol formation, the critical challenge involves the chemical speciation of nucleation precursors and disentangling the corresponding nucleating mechanism at the molecular level[5,6].

Globally, marine NPF are significantly influenced by biogenic emissions, although anthropogenic impacts are also involved, to a lesser extent, especially in the remote ocean[7]. Field observations have shown that marine NPF is closely related to the iodine-bearing molecules[8], which originate from iodine vapors emitted by marine algal[9,10]. Among these iodine components, iodic acid (HIO_3, IA) has been identified to be the key NPF driver in the coastal, open ocean, and ice-covered polar regions[11–13]. However, atmospheric observations of IA cannot be associated with predicted particle formation rates[14]. Given the complexity of atmospheric components, other widespread precursors over the oceans, especially from biological emissions, may also be involved in the formation process of IA particles. Amines (e.g., mono-methylamine MA, dimethylamine DMA, and trimethylamine TMA), as nitrogenous bases widely distributed in the atmosphere[15], possess relatively strong basicity and consequently stabilization effect on acidic nucleation precursors such as well-known sulfuric acid (SA)[15,16] and methanesulfonic acid (MSA)[17,18]. As the stronger stabilizer of these amine molecules (DMA ≥ TMA > MA)[16], the most extensively studied DMA has been identified as a major nucleating precursor in the coastal city of Shanghai, China[19], coastal

California[20], and over the open ocean[21,22]. Moreover, the widespread DMA has a considerable atmospheric concentration (0.4–10 pptv) over the ocean, making it important for marine NPF[23]. Considering the ability of DMA to efficiently stabilize acidic precursors and its wide distribution in the marine atmosphere[24–27], there is a potential for DMA to stabilize IA molecules via acid-base reactions. However, whether DMA is capable of rapid clustering with IA and the corresponding nucleation process are unknown at the molecular level.

To investigate the nucleation process of IA and DMA, the combination of a quantum chemical method with Atmospheric Clusters Dynamic Code (ACDC)[28] were employed to simulate the nucleation kinetic process. A multi-step conformational search was systematically performed to identify stable conformations of $(IA)_x \cdot (DMA)_y$ ($1 \le x \le 6$, $1 \le y \le 3$, $x + y \le 6$) clusters with global minima energy. The nature of IA binding with DMA within the cluster was studied by wavefunction analysis, and cluster thermodynamic properties are calculated to assess the stability of clusters. To further study IA-DMA nucleation under different marine areas, a series of ACDC simulations were carried out at the corresponding atmospheric conditions (varying precursor concentrations and temperatures). Furthermore, to characterize the role of DMA in stabilizing IA clusters, the corresponding molecular-level nucleating mechanism was further proposed by tracking the clustering pathways.

RESULTS

Cluster conformation

Strong intermolecular interactions are essential for the formation of stable molecular clusters. To evaluate the binding potential

[1]Key Laboratory of Cluster Science, Ministry of Education of China, School of Chemistry and Chemical Engineering, Beijing Institute of Technology, Beijing 100081, China. [2]Atmospheric Sciences Research Center, University at Albany, Albany, New York, NY 12203, USA. [3]Environment Research Institute, Shandong University, Qingdao 266237, China. [4]State Key Laboratory for Structural Chemistry of Unstable and Stable Species, CAS Research/Education Center for Excellence in Molecular Sciences, Institute of Chemistry, Chinese Academy of Sciences, Beijing 100190, China. ✉email: zhangxiuhui@bit.edu.cn
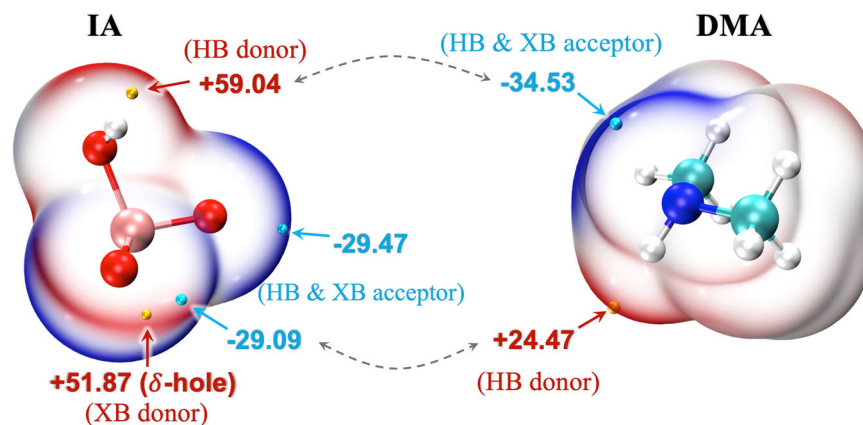
Fig. 1 The ESP-mapped molecular vdW surfaces of iodic acid (IA) and dimethylamine (DMA). The golden and cyan dots indicate the positions of maximums and minimums of ESP in kcal mol^{-1}, respectively. The gray dashed arrows refer to the tendencies of site-to-site interactions. HB (Hydrogen bond), XB (Halogen bond); The pink, red, cyan, blue, and silver spheres represent I, O, C, N, and H atoms, respectively.

between IA and DMA, their possible interaction sites were first analyzed through the electrostatic surface potential (ESP) in Fig. 1, where the red electron-deficient region tends to attract the blue electron-rich region. As illustrated in Fig. 1, IA has a positive ESP maximum ($+59.04$ kcal mol^{-1}) at the H atom of its -OH group, which can act as a hydrogen bond (HB) donor. And there is an ESP minimum (-29.09 kcal mol^{-1}) at the terminal oxygen atom in IA, mainly attributed to its lone pair electrons, making it available as an HB acceptor. As to DMA, the -NH group can serve as both HB donor and acceptor.

In this case, hydrogen bonding between IA and DMA results in the formation of a heterodimer (IA)$_1$·(DMA)$_1$ (Fig. 2). In addition to HB, IA also potentially forms halogen bonds (XB) with DMA or itself via its XB donor site (δ-hole with ESP value of $+51.87$ kcal mol^{-1}) with the -NH group in DMA (XB acceptor).

Figure 2 presents the identified (IA)$_x$·(DMA)$_y$ ($1 \leq x \leq 6$, $1 \leq y \leq 3$, $2 \leq x + y \leq 6$) clusters with lowest free energies. Within these clusters, IA and DMA are structurally stabilized by the network built with HBs (black dashed lines) and XBs (green dashed lines). Moreover, the acid-base reactions occurred during cluster formation, accompanied by the proton transferring from IA to DMA. Among these IA-DMA clusters, proton transfer between IA and DMA occurred within all clusters except for the (IA)$_{1-2}$·(DMA)$_3$ clusters, and the binding sites of the unprotonated DMA were all involved in forming HBs or XBs. Specifically, HBs within IA-DMA clusters exist in four forms, in the order of number: N-H···O (79%) > O-H···O (13%) > O-H···N (5%) > N-H···N (3%). The high percentage of N-H···O is due to the N-H covalent bonds formed by proton transfer (O-H···N → O···H-N) within most IA-DMA clusters.

For HB strength, according to the AIM calculation (Supplementary Table 1), the Laplacian electron density $\nabla^2\rho(r)$ at the BCPs is in the range of 0.0469–0.1689 (a.u.), and energy density $H(r)$ is -0.0250–0.0023 (a.u.). Further, based on the classification of HBs[29], most of the formed HBs (79%) belong to medium HBs (12.0 < binding energy < 24.0 kcal mol^{-1}) with $\nabla^2\rho(r) > 0$ and $H(r)$ < 0. And for XBs within clusters, O-I···O contributes more (84%) than O-I···N XBs (16%), acting mainly between IA molecules. Overall, IA-DMA clusters are jointly stabilized by multiple types of intermolecular HBs and XBs. Also, during the clustering process, the acid-base reactions between IA and DMA occur in most clusters, resulting in acid-base ion pairs.

Cluster stability
To further evaluate the thermodynamic stability of clusters, the Gibbs formation free energies (ΔG) of the studied clusters were

calculated at the condition of $T = 218$–298 K and $p = 1$ atm (Supplementary Tables 2, 3). Figure 3a presents the ΔG at 278 K of (IA)$_x$·(DMA)$_y$ ($0 \leq x \leq 6$, $0 \leq y \leq 3$, $1 \leq x + y \leq 6$) clusters. Compared with pure (IA)$_{2-6}$ clusters, the (IA)$_{1-5}$·(DMA)$_1$ clusters possess 8.01–16.56 kcal mol^{-1} lower ΔGs, indicating greater cluster thermodynamic stability enhanced by DMA. Moreover, for IA-DMA clusters with the same number of molecules, the ΔG of the cluster with more acid and less base is significantly lower than that of the cluster with more base and less acid. Furthermore, the stabilization effect of DMA on IA was compared with that of another important atmospheric nitrogenous base molecule, NH$_3$, as shown in Fig. 3. Taken as a whole, the ΔGs of IA-DMA clusters are 8.04–27.08 kcal mol^{-1} lower than those of the corresponding IA-NH$_3$ clusters. Moreover, the total evaporation rates ($\Sigma\gamma$ in s^{-1} at 278 K) of most IA-DMA clusters presented in Fig. 3b are also lower than those of IA-NH$_3$ clusters, except for the (IA)$_{1-2}$·(DMA)$_3$ clusters, probably due to the steric hindrance effect caused by three unprotonated DMA (Supplementary Fig. 1). The lower $\Sigma\gamma$ and higher $\beta C/\Sigma\gamma$ (Supplementary Fig. 2) of IA-DMA clusters further reflect their stronger cluster stability than IA-NH$_3$ clusters. The detailed cluster evaporation paths and the corresponding γ at 278 K are collected in Supplementary Table 4.

Furthermore, considering the difference in atmospheric concentrations of DMA and NH$_3$, the actual Gibbs free energy affected by vapor concentration[30] was calculated by Eq. (3) and shown in Fig. 3c. For the pure-IA system (blue line), the clustering process by sequential addition of IA monomer needs to cross an energy barrier of 10.59 kcal mol^{-1} at conditions of [IA] = 10^8 molecules cm^{-3}. As to the IA-NH$_3$ system (yellow line), the addition of NH$_3$ can reduce the energy barrier to 6.46 kcal mol^{-1} at [NH$_3$] = 400 pptv (median value)[31]. While for the IA-DMA system, the proposed IA-DMA clustering path (red lines), in which the (IA)$_{2-4}$·(DMA)$_2$ and (IA)$_{1-5}$·(DMA)$_1$ clusters dominate, is a barrierless process even at its lower concentration ([DMA] = 0.4 pptv)[23]. Overall, the IA-DMA clustering pathway is more energetically favorable than the pure-IA and IA-NH$_3$ systems (Supplementary Fig. 3), and the formed IA-DMA clusters have greater stability.

Cluster formation rate
To further study the IA-DMA nucleation kinetics, the steady-state cluster formation rate J (cm^{-3} s^{-1}) were simulated by ACDC at ambient conditions of $T = 278$ K and condensation sink coefficient (CS) of 2.0×10^{-3} s^{-1} for coastal region[32]. In the simulations, the employed IA monomer concentration ([IA]) here is the total concentration of clusters consisting of one IA and any number of base, corresponding to the measurable acid concentration.
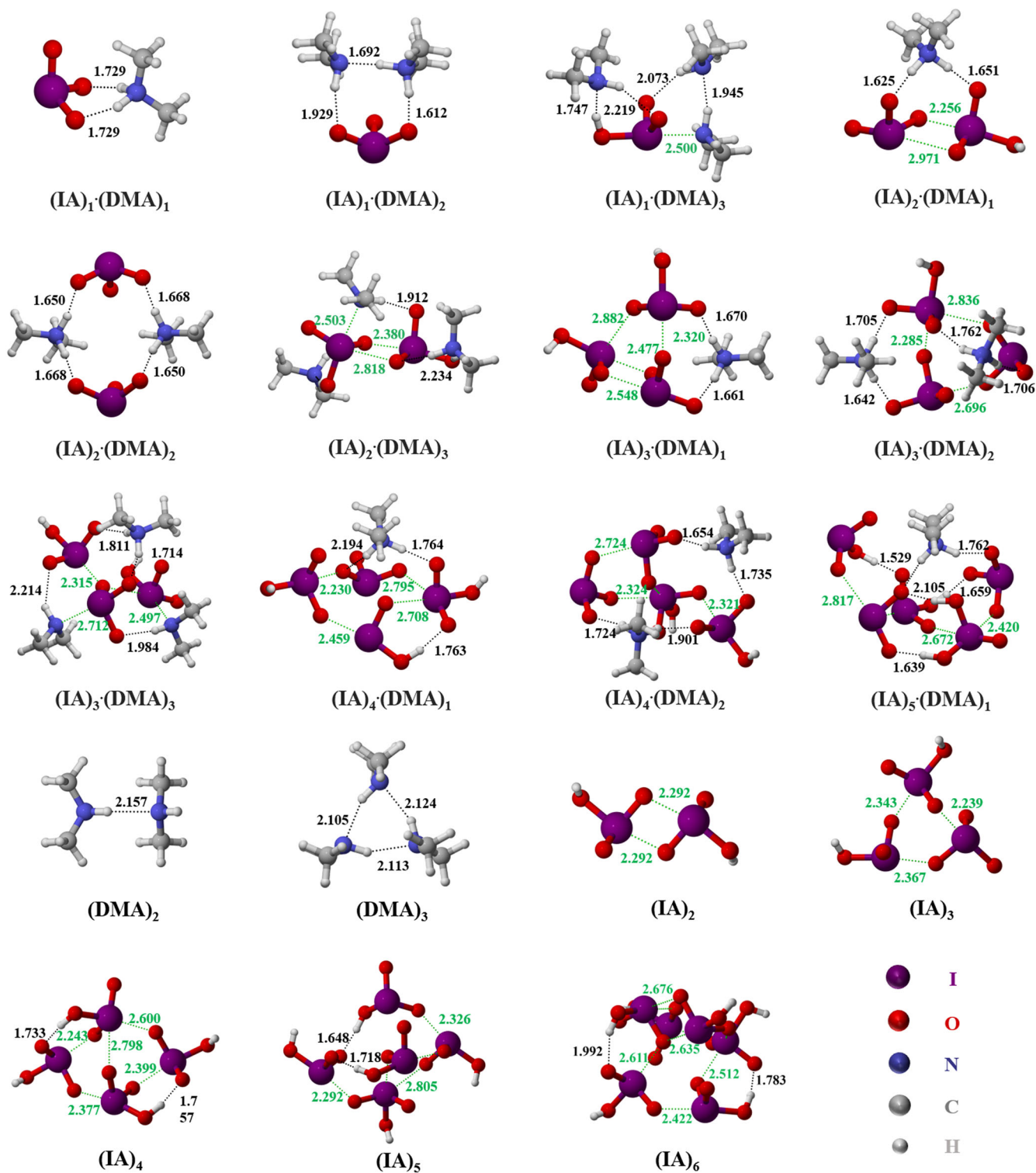
Fig. 2 The most stable cluster configurations. The $(IA)_x \cdot (DMA)_y$ ($1 \le x \le 6$, $1 \le y \le 3$, $2 \le x + y \le 6$) clusters with lowest Gibbs formation free energies at the ωB97XD/6-311++G(3df, 3pd) (for C, H, O, N atoms) + aug-cc-pVTZ-PP with ECP28MDF (for I atom) level of theory. The black and green dashed lines indicate the formed HBs and XBs, respectively. The lengths of bonds are given in Å.

Figure 4 presents J of the pure-IA (blue line), IA-NH$_3$ (yellow area), and IA-DMA systems (red area) at the corresponding precursor concentrations over the oceans: [IA] = $10^6 \sim 10^8$ (molecules cm^{-3})[12], [DMA] = 0.01~10 pptv[23,33] and [NH$_3$] = 40~10^3 pptv[31,34]. As shown in Fig. 4, compared with pure-IA nucleation, the involvement of both DMA and NH$_3$ in clustering significantly

promote the rate J, indicating that both have an enhancement effect on the formation of IA clusters. Interestingly, the far lower [DMA] (0.01~10 pptv) relative to [NH$_3$] (40~10^3 pptv) can promote J to a higher level (red area), indicating that the formation of IA-involved particles is more sensitive to the enhancement effects of DMA. It is worth noting that the enhancement of DMA on J
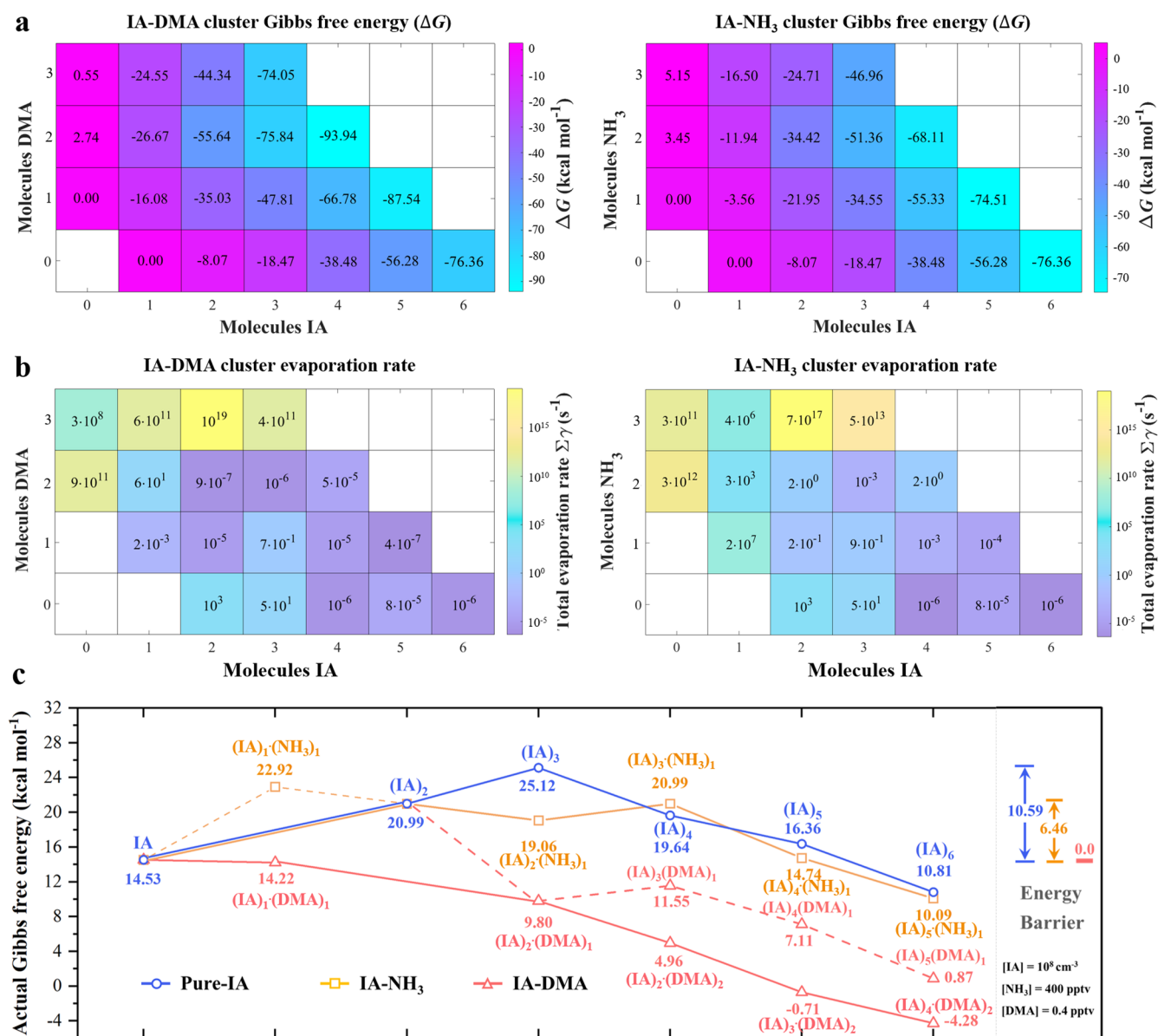
a

IA-DMA cluster Gibbs free energy (ΔG)

IA-NH$_3$ cluster Gibbs free energy (ΔG)

b

IA-DMA cluster evaporation rate

IA-NH$_3$ cluster evaporation rate

c

Fig. 3 Comparison of IA-DMA and IA-NH3 cluster properties. a Gibbs formation free energies (ΔG) of the $(IA)_x \cdot (DMA)_y$ and $(IA)_x \cdot (NH_3)_y$ ($0 \leq x \leq$ 6, $0 \leq y \leq 3$, $x + y \leq 6$) clusters at the RI-CC2/aug-cc-pVTZ-PP//ωB97XD/6-311++G(3df,3pd) + aug-cc-pVTZ-PP level of theory, $T = 278$ K, and $p = 1$ atm. **b** the total evaporation rates ($\Sigma \gamma$ in s^{-1}) and **c** the actual Gibbs free energy (Eq. 3) of the corresponding clusters. The solid and dashed lines represent the primary and secondary paths, respectively.

increases with [DMA], but dulling occurs for [DMA] greater than 1 pptv (Supplementary Fig. 7). Although the adopted [DMA] is three orders of magnitude lower than [NH$_3$], the resulting J of IA-DMA system is still higher than that of IA-NH$_3$. Further comparison (Supplementary Fig. 8) reveals that the J of IA-DMA nucleation can better match the field observations in Mace Head[12] and Zhejiang[8]. Accordingly, the proposed efficient IA-DMA nucleation may help to explain some intensive marine NPF events with rapid IA cluster formation.

Cluster formation pathway

To further reveal the mechanism of nucleation kinetics, the cluster formation pathways of the IA-DMA system were tracked at the molecular level by ACDC (Fig. 5a). Kinetic simulations were performed under the conditions of $T = 278$ K, CS $= 2 \times 10^{-3}$ s^{-1}, [IA] $= 10^8$ (molecules cm^{-3})[12], and [DMA] $= 0.01 \sim 10$ pptv[23,33]. As

shown in Fig. 5a, the cluster formation pathways can be divided into two categories: (i) the pure-IA self-nucleation and (ii) IA-DMA-based cluster formation. For the pure-IA pathway, the cluster growth proceeds mainly via the sequential addition of IA monomer, which is consistent with the findings of the previous study[35]. And for the IA-DMA pathway proposed in this study, DMA first binds with IA to form a heterodimer $(IA)_1 \cdot (DMA)_1$. Next, the formed $(IA)_1 \cdot (DMA)_1$ cluster continues growing by the addition of IA to form $(IA)_2 \cdot (DMA)_1$ cluster. The $(IA)_2 \cdot (DMA)_1$ cluster further collides with DMA monomer and $(IA)_1 \cdot (DMA)_1$ to form $(IA)_2 \cdot (DMA)_2$ and $(IA)_3 \cdot (DMA)_2$ clusters, respectively. Subsequently, the cluster growth is mainly through the continuous addition of IA monomers, resulting in larger $(IA)_{3-4} \cdot (DMA)_2$ and $(IA)_{4-5} \cdot (DMA)_1$ clusters. Finally, the formed $(IA)_{3-4} \cdot (DMA)_2$ and $(IA)_5 \cdot (DMA)_1$ can further bind with IA monomer or IA-containing cluster to grow out of the simulated system. Under different conditions, as shown in Fig. 5b, different out-growing paths contribute differently to J.
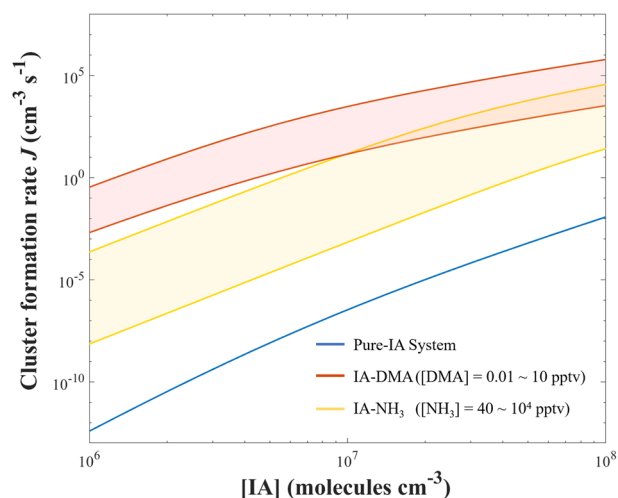
Fig. 4 Simulated cluster formation rates J ($cm^{-3}s^{-1}$). J as a function of IA concentration of Pure-IA, IA-DMA, and IA-NH$_3$ system at $T = 278$ K and CS $= 2.0 \times 10^{-3}$ s^{-1}.

At low [DMA] (0.01 pptv), flux out from (IA)$_5$·(DMA)$_1$ dominates (65%). And at [DMA] of 0.1~1.0 pptv, the cluster growth based on (IA)$_4$·(DMA)$_2$ contributes the most (72%). And when [DMA] increases to 10 pptv, cluster formation is mainly affected by the formation of (IA)$_3$·(DMA)$_2$ clusters colliding with other clusters. Moreover, to assess the contribution of each cluster to the particle formation, the steady-state number concentrations of all studied clusters were calculated at $T = 278$ K, [IA] $= 10^8$ molecules and [DMA] $= 0.4$ pptv. As shown in Fig. 5c, the concentration of most DMA-containing clusters (blue cycle), such as (IA)$_{1-5}$·(DMA)$_1$ and (IA)$_{2-4}$·(DMA)$_2$, is higher than that of pure-IA clusters (red cycle), due to the greater stability of IA-DMA clusters (recall Section 3.2). For the total particle concentration, the IA-DMA nucleating pathway (blue line along (IA)$_{1-5}$·(DMA)$_1$ and (IA)$_{2-4}$·(DMA)$_2$ clusters) contributes more than that of the IA self-nucleation (red line along (IA)$_{2-6}$ clusters). In the largest clusters (IA)$_4$·(DMA)$_2$, (IA)$_5$·(DMA)$_1$, and (IA)$_6$ with outgrowth potential (Supplementary Methods), the ratios of IA to DMA were calculated in Supplementary Fig. 9 by weighting their steady-state concentrations at varying [IA] (10^6~ 10^8 molecules cm^{-3}) and [DMA] (0.01~10 pptv). The resulting ratio of IA/DMA in these clusters is 2.0~ 3.5, indicating that IA is still the main cluster component (67–78%). Overall, the IA-DMA clusters contribute more to the nucleating process than the pure-IA clusters. Although DMA is a minor component of the formed IA-DMA cluster, it does play a key role in enhancing IA cluster formation. Accordingly, these stable IA-DMA clusters may provide a large number of seeds for the marine NPF.

Atmospheric impact of IA-DMA system

To quantify the promotion of DMA on IA cluster formation, we thus defined the enhancement strength as R in Eq. (1):

$$R = \frac{J([IA] = x, [DMA] = y)}{J([IA] = x)} \quad (1)$$

where x and y are the gaseous concentrations of IA and DMA, respectively.

Atmospheric conditions vary with regions and seasons, which in turn sway the influence of the IA-DMA mechanism. Herein, as shown in Fig. 6, the enhancement of DMA on IA cluster formation was simulated in different marine regions with the corresponding ambient conditions.

In the ACDC simulation, the average temperature data for each month (orange lines) at different locations was taken from the NASA database[36], the [IA] were set with reference to the reported

field observations[14], and the [DMA] were set based on the GEOS-Chem simulations[33], where the specific values at different sites and moths were determined by the latitude and longitude of the studied sites. For mid-latitude oceans, CS is set to be a typical value (2.0×10^{-3} s^{-1}) of coastal regions[32] for Mace Head, 1.0×10^{-2} s^{-1} for Zhejiang[8], and for other high-latitude polar regions, CS is set to be 1.0×10^{-4} (s^{-1})[14].

The results indicate that R is positively correlated with the temperature (T) at each site. As shown in Fig. 6a–c, R is higher during the summer months in the northern and southern hemispheres. Specifically, in coastal areas of the northern hemisphere, such as Mace head, Zhejiang, and Ny-Ålesund, the enhancement R of DMA on IA cluster formation (Green pillars) is relatively stronger in June–August. While in the southern hemisphere offshore regions, such as Réunion, Aboa, and Neumayer (Fig. 6d–f), the higher R occurs in November–March. The reason for this phenomenon is that J of the pure-IA system (denominator of R) is more sensitive to T than that of the IA-DMA system (the numerator of R) (Supplementary Fig. 6). In addition to T, varying [IA] and [DMA] also affect R to a greater or lesser extent. From the definition of enhancement R (Eq. (1)), the [IA] affects both numerator (J_{IA-DMA}) and denominator ($J_{pure-IA}$) simultaneously, and thus has a relatively small effect on their ratio (R). In contrast, although [DMA] has a greater effect on R, as it only affects the J_{IA-DMA} (the numerator of R), it still does not present any correlation with R.

In summary, the effects of the IA-DMA mechanism vary with the ambient conditions of different marine regions. It shows a clear seasonal feature mainly influenced by temperature all year round, specifically the enhancement of DMA on IA cluster formation rate can be more than five orders of magnitude, which is stronger in summer. This enhancement effect of DMA is relatively stronger in the northern hemisphere oceans, due to the relatively richer DMA, than in the southern hemisphere.

DISCUSSION

Iodic acid (IA) has been identified as an essential driver for marine NPF. As an essential stabilizer of atmospheric acidic precursors, dimethylamine (DMA) potentially stabilizes IA clusters via acid-base reactions. Hence, in this study, we have investigated the (IA)$_x$(DMA)$_y$ ($1 \le x \le 6$, $1 \le y \le 3$, $x + y \le 6$) nucleating system using the density functional theory (DFT) and Atmospheric Cluster Dynamics Code (ACDC). Results indicate that DMA can stabilize IA via hydrogen and halogen bonding, and the clustering process is energy barrierless. The formed IA-DMA clusters are more stable than pure-IA and IA-NH$_3$ clusters. Moreover, DMA can significantly promote the formation of IA clusters stemming from the resulting boosted J, especially in summer, and its promotion efficiency is much higher than that of NH$_3$.

In the revealed IA-DMA nucleating pathways, the clustering process is dominated by the more stable IA-DMA clusters rather than the sequential addition of IA. Overall, DMA potentially plays a critical role in enhancing IA cluster stability, and thus formation rates. The uncovered IA-DMA nucleation mechanism may help to reveal some missing sources of fresh particles and thus better understand intensive marine NPF events. Considering the relatively short lifetime of DMA, the IA-DMA nucleation is especially effective in a hot-spot NPF event near their emission sources.

Considering the complexity of the marine atmosphere, many factors might affect the nucleation process of IA and DMA, such as the humidity effect. The effect of water was not considered here because of its weak ability to bind IA[37] and the hydrogen bonds formed by water are weaker than those between acid and base precursors[38]. Nevertheless, the humidity effect on the nucleating process in regions with sparse IA and DMA still needs to be considered in future. In addition, the influence of other important nucleation precursors such as sulfuric acid (H$_2$SO$_4$),
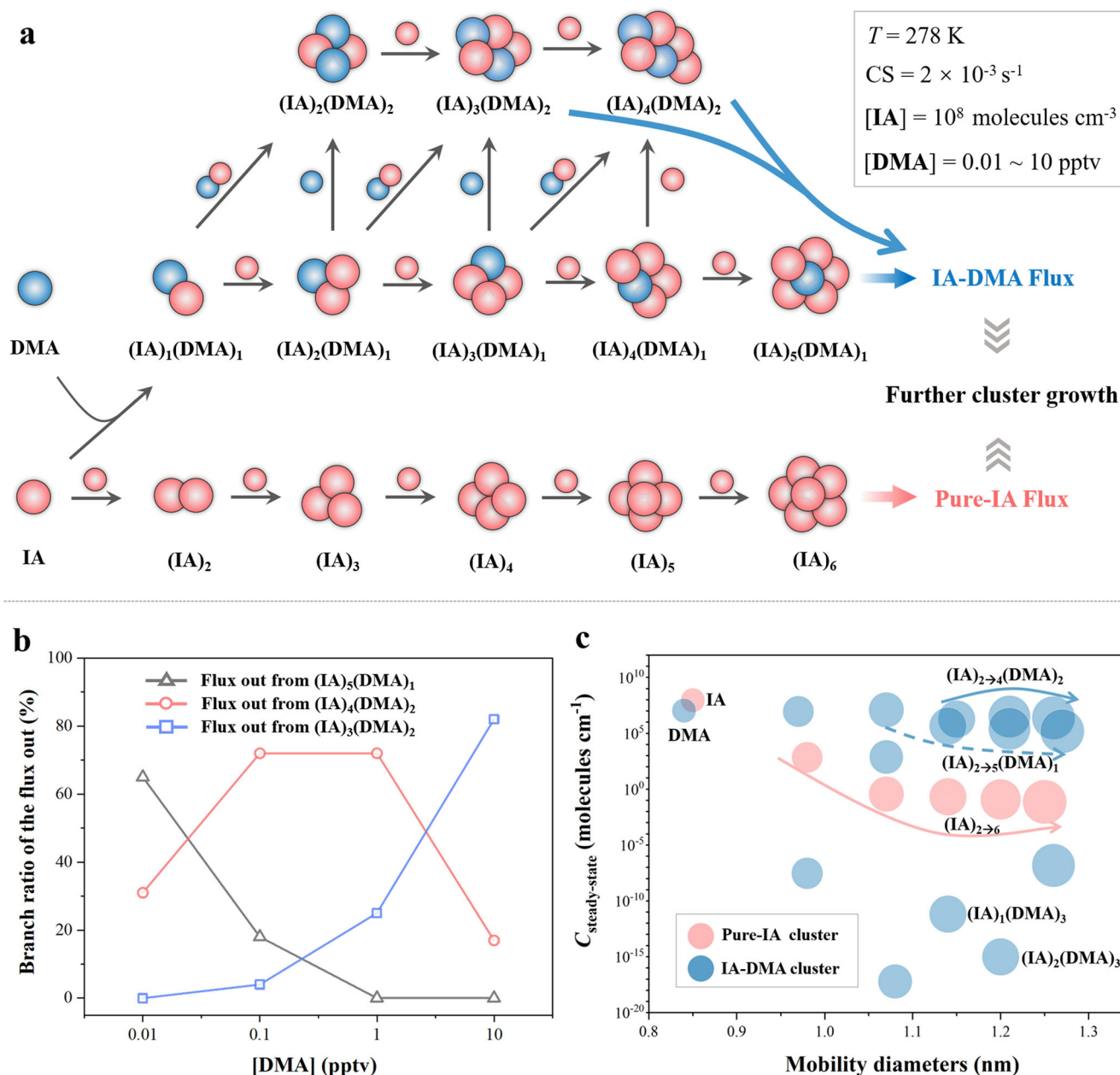
Fig. 5 Cluster formation pathways and the corresponding contributions. a Cluster formation pathway of IA-DMA system under the condition of $T = 278$ K, $CS = 2 \times 10^{-3}$ s^{-1}, [IA] $= 10^8$ molecules cm^{-3}, and [DMA] $= 0.01$~10 pptv. **b** Branch ratio of the flux out (%) against different [DMA]. **c** Steady-state cluster concentrations against cluster mobility diameters (D_M, nm), where the circle size is proportional to the D_M. The red and blue arrows correspond to the pure-IA and IA-DMA clustering pathways in **a**, respectively.

methanesulfonic acid (CH_4O_3S), or iodine oxide, which potentially coexist in the marine atmosphere, should also be considered in future studies.

METHODS

Quantum chemistry calculations

To fully sample the isomers of each studied IA-DMA cluster, the systematic multi-step conformation search was adopted here to obtain the cluster structures with minimum energy (Supplementary Methods). The final lowest-lying structure were optimized at ωB97XD/6-311++G(3df,3pd) (for C, H, O, N) + aug-cc-pVTZ-PP with ECP28MDF (for I) level of theory[39,40]. In addition to IA-DMA clusters, the employed IA-NH$_3$ cluster structures were referred to the previous studies[35,41] and reoptimized at the employed level of

theory in this study. The structures with lower Gibbs free energies were retained and the corresponding Cartesian coordinates are summarized in Supplementary Table 5. All structural optimizations with tight convergence criteria (Integration grid: FineGrid) and frequency calculations were performed by density functional theory (DFT) using Gaussian 09 program[42].

Furthermore, the single-point correction was performed by RI-CC2 method[43] with aug-cc-pVTZ[44] (for C, H, O, N) + aug-cc-pVTZ-PP with ECP28MDF (for I) basis set[45] using Turbomole program[46], since there is evidence that ACDC simulations based on RI-CC2 values are in better agreement with the experimental results[47–49]. Herein, in the present work, the Gibbs formation free energy (ΔG) of the IA-DMA and IA-NH$_3$ cluster is calculated as Eq. (2):

$$\Delta G = \Delta E_{\text{RI-CC2}} + \Delta G_{\text{thermal}}^{\omega\text{B97X-D}} \quad (2)$$
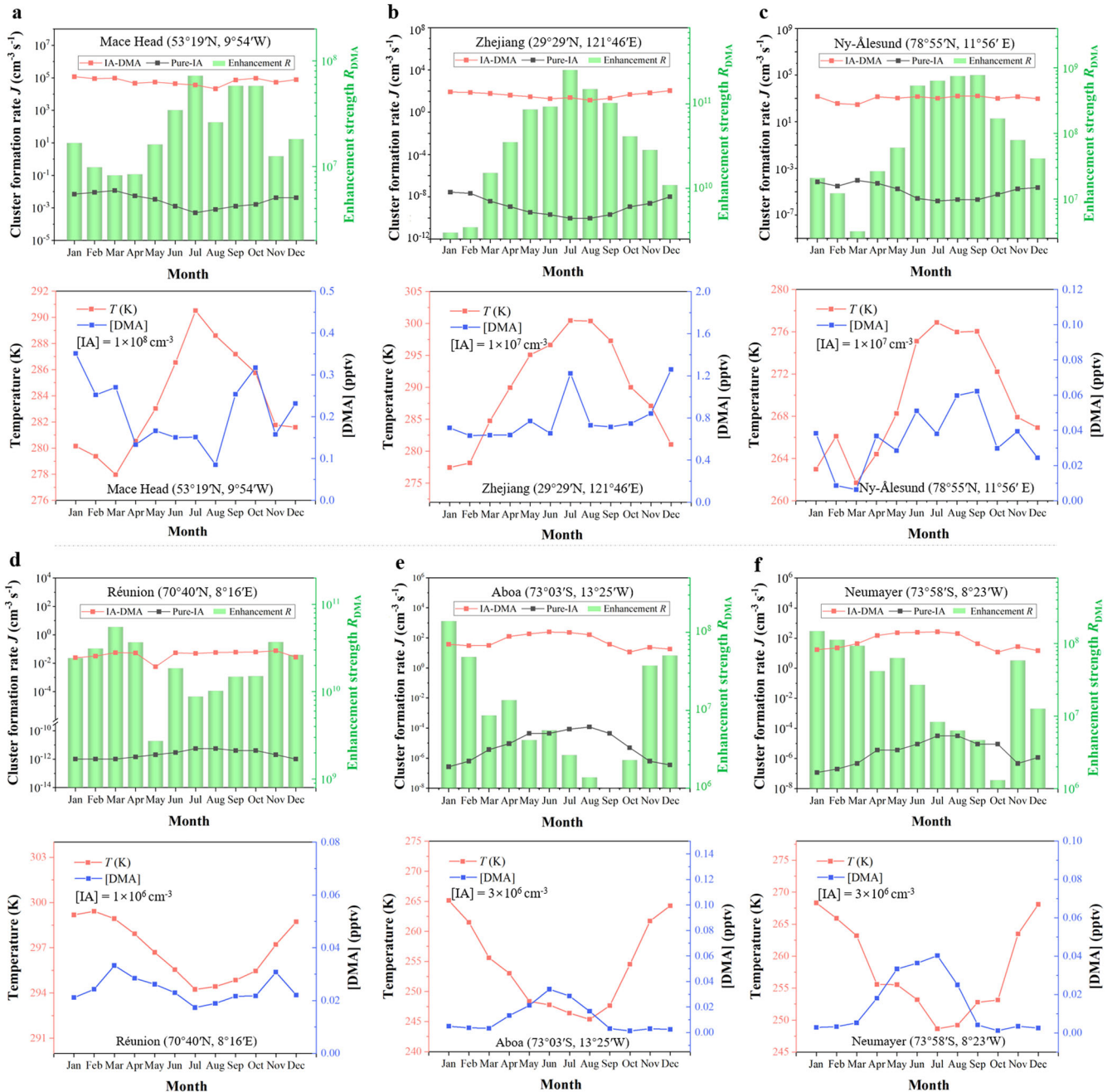
Fig. 6 The IA-DMA nucleation in different regions. Cluster formation rates (J, cm^{-3} s^{-1}) shown in orange squares (IA-DMA) and black squares (pure-IA) and the enhancement R by DMA (Green pillars) at varying atmospheric conditions in different months of **a** Mace Head, **b** Zhejiang, **c** Ny-Ålesund, **d** Réunion, **e** Aboa, and **f** Neumayer.

where $\Delta G_{thermal}$ is the thermal contribution and ΔE is the electronic contribution to Gibbs free energy. To simulate nucleation at varying temperatures, the ΔG of IA-DMA clusters at $T = 218–298$ K were calculated by Shermo[50] and collected in Supplementary Table 2. In addition, considering the effect of vapor concentration[30], the actual Gibbs free energy was also calculated as Eq. (3):

$$\Delta G(P_1, P_2, ..., P_n) = \Delta G_{ref} - k_B T \sum_{i=1}^{n} N_i \ln\left(\frac{P_i}{P_{ref}}\right) \quad (3)$$

where ΔG_{ref} is calculated at the reference pressure P_{ref} (1 atm), k_B is the Boltzmann constant, n is the number of components in the cluster, N_i is the number of molecules i within the cluster and P_i is the partial pressure of component i.

Wavefunction analysis

Intermolecular interactions can intrinsically affect the stability of the formed cluster. Hence, to better understand the binding nature, the identified cluster structure was investigated by wavefunction analysis using Multiwfn 3.8[51]. Specifically, the electrostatic potential (ESP) on the molecular vdW surface was calculated to identify potential interaction sites. The reduced density gradient (RDG)[52] analysis was conducted to characterize

non-covalent interactions. To further quantify the strength of interactions, electron density $\rho(r)$, Laplacian electron density $\nabla^2\rho(r)$, energy density $H(r)$ at corresponding bond critical points (BCPs) based on atoms in molecules (AIM) theory[53] were also calculated in this study (Supplementary Table 1).

Atmospheric cluster dynamic simulations

The Atmospheric Clusters Dynamic Code (ACDC)[28] derives the steady-state concentration and cluster formation rates by solving the birth-death equation (Eq. (4) as below) of the studied clusters. For each ACDC simulation, all possible collision and evaporation processes were considered in this study.

$$\frac{dC_i}{dt} = \frac{1}{2}\sum_{j<i}\beta_{j,(i-j)}C_jC_{(i-j)} + \sum_j\gamma_{(i+j)\to i}C_{i+j} \\ - \sum_j\beta_{i,j}C_iC_j - \frac{1}{2}\sum_{j<i}\gamma_{i\to j}C_i + Q_i - S_i \quad (4)$$

where $\beta_{i,j}$ is the collision rate coefficient between clusters i and j, C_i is the concentration of cluster i, $\gamma_{i,j}$ is the evaporation rate coefficient of a cluster $(i+j)$ evaporating into smaller clusters i and j, Q_i is an outside source term of cluster i, and S_i is the other possible sink term of cluster i. Details for calculating $\beta_{i,j}$ and $\gamma_{i,j}$ is presented in Supplementary Methods.

In the ACDC simulations, the growth of clusters out of the simulated system depends on whether the rate at which clusters collide with monomers exceeds their own evaporation ($\beta C/\sum\gamma$ >1)[54]. Once the boundary clusters (the smallest ones out of the system) are formed, they tend to keep growing without evaporating into smaller sizes[28]. Here, the boundary clusters in the IA-DMA system are set to be $(IA)_7$, $(IA)_5\cdot(DMA)_2$ and $(IA)_6\cdot(DMA)_1$ clusters (see Supplementary Methods). For the IA-NH$_3$ system, the boundary clusters are set to be $(IA)_7$ and $(IA)_6\cdot(NH_3)_1$ clusters with reference to previous study[35]. Moreover, the effect of different condensation sink coefficients (1.0×10^{-2}–$1.0 \times 10^{-4}\,s^{-1}$), covering coastal to polar regions[8,14,32], on the results was examined in Supplementary Figs. 4, 5.

DATA AVAILABILITY

All data were available in the main text or supplementary materials. All other relevant data are available from the corresponding authors upon reasonable request.

CODE AVAILABILITY

ACDC code is publicly available at https://github.com/tolenius/ACDC.

REFERENCES

1. Collins, M. et al. Long-term climate change: projections, commitments and irreversibility. in Climate Change 2013-The Physical Science Basis: Contribution of Working Group I to the Fifth Assessment Report of the Intergovernmental Panel on Climate Change 1029–1136 (Cambridge University Press, 2013).
2. Takegawa, N. et al. Enhanced New Particle Formation Above the Marine Boundary Layer Over the Yellow Sea: Potential Impacts on Cloud Condensation Nuclei. J. Geophys. Res. Atmos. 125, (2020).
3. Kulmala, M. How particles nucleate and grow. Science 302, 1000–1001 (2003).
4. Kulmala, M. et al. Direct observations of atmospheric aerosol nucleation. Science 339, 943–946 (2013).
5. O'Dowd, C. D. & de Leeuw, G. Marine aerosol production: a review of the current knowledge. Philos. Trans. R. Soc. A. 365, 1753–1774 (2007).
6. Zhang, R., Khalizov, A., Wang, L., Hu, M. & Xu, W. Nucleation and growth of nanoparticles in the atmosphere. Chem. Rev. 112, 1957–2011 (2012).
7. Kerminen, V.-M. et al. Atmospheric new particle formation and growth: review of field observations. Environ. Res. Lett. 13, 103003 (2018).

8. Yu, H. et al. Iodine speciation and size distribution in ambient aerosols at a coastal new particle formation hotspot in China. Atmos. Chem. Phys. 19, 4025–4039 (2019).
9. McFiggans, G. et al. Direct evidence for coastal iodine particles from Laminaria macroalgae – linkage to emissions of molecular iodine. Atmos. Chem. Phys. 4, 701–713 (2004).
10. Saiz-Lopez, A. et al. Atmospheric chemistry of iodine. Chem. Rev. 112, 1773–1804 (2012).
11. Baccarini, A. et al. Frequent new particle formation over the high Arctic pack ice by enhanced iodine emissions. Nat. Commun. 11, 4924 (2020).
12. Sipilä, M. et al. Molecular-scale evidence of aerosol particle formation via sequential addition of HIO3. Nature 537, 532–534 (2016).
13. Beck, L. J. et al. Differing mechanisms of new particle formation at two arctic sites. Geophys. Res. Lett. 48, e2020GL091334 (2021).
14. He, X.-C. et al. Role of iodine oxoacids in atmospheric aerosol nucleation. Science 371, 589–595 (2021).
15. Almeida, J. et al. Molecular understanding of sulphuric acid-amine particle nucleation in the atmosphere. Nature 502, 359–363 (2013).
16. Olenius, T. et al. New particle formation from sulfuric acid and amines: comparison of monomethylamine, dimethylamine, and trimethylamine. J. Geophys. Res. Atmos. 122, 7103–7118 (2017).
17. Bork, N., Elm, J., Olenius, T. & Vehkamäki, H. Methane sulfonic acid-enhanced formation of molecular clusters of sulfuric acid and dimethyl amine. Atmos. Chem. Phys. 14, 12023–12030 (2014).
18. Shen, J. et al. Structural effects of amines in enhancing methanesulfonic acid-driven new particle formation. Environ. Sci. Technol. 54, 13498–13508 (2020).
19. Yao, L. et al. Atmospheric new particle formation from sulfuric acid and amines in a Chinese megacity. Science 361, 278–281 (2018).
20. Youn, J.-S., Crosbie, E., Maudlin, L. C., Wang, Z. & Sorooshian, A. Dimethylamine as a major alkyl amine species in particles and cloud water: Observations in semi-arid and coastal regions. Atmos. Environ. 122, 250–258 (2015).
21. Facchini, M. C. et al. Important source of marine secondary organic aerosol from biogenic amines. Environ. Sci. Technol. 42, 9116–9121 (2008).
22. Brean, J. et al. Open ocean and coastal new particle formation from sulfuric acid and amines around the Antarctic Peninsula. Nat. Geosci. 14, 383–388 (2021).
23. van Pinxteren, M. et al. Aliphatic amines at the Cape Verde atmospheric observatory: abundance, origins and sea-air fluxes. Atmos. Environ. 203, 183–195 (2019).
24. Grönberg, L., Lövkvist, P. & Jönsson, J. Å. Measurement of aliphatic amines in ambient air and rainwater. Chemosphere 24, 1533–1540 (1992).
25. Van Neste, A., Duce, R. A. & Lee, C. Methylamines in the marine atmosphere. Geophys. Res. Lett. 14, 711–714 (1987).
26. Gibb, S. W., Mantoura, R. F. C. & Liss, P. S. Ocean-atmosphere exchange and atmospheric speciation of ammonia and methylamines in the region of the NW Arabian Sea. Glob. Biogeochem. Cycles 13, 161–178 (1999).
27. Quéléver, L. L. J. et al. Investigation of new particle formation mechanisms and aerosol processes at Marambio Station, Antarctic Peninsula. Atmos. Chem. Phys. 22, 8417–8437 (2022).
28. McGrath, M. J. et al. Atmospheric cluster dynamics code: a flexible method for solution of the birth-death equations. Atmos. Chem. Phys. 12, 2345–2355 (2012).
29. Rozas, I., Alkorta, I. & Elguero, J. Behavior of ylides containing N, O, and C atoms as hydrogen bond acceptors. J. Am. Chem. Soc. 122, 11154–11161 (2000).
30. Vehkamäki, H. Classical Nucleation Theory in Multicomponent Systems (Springers, 2006).
31. Wentworth, G. R. et al. Ammonia in the summertime Arctic marine boundary layer: sources, sinks, and implications. Atmos. Chem. Phys. 16, 1937–1953 (2016).
32. Dal Maso, M. et al. Condensation and coagulation sinks and formation of nucleation mode particles in coastal and boreal forest boundary layers. J. Geophys. Res Atmos. 107, PAR 2-1–PAR 2-10 (2002).
33. Yu, F. & Luo, G. Modeling of gaseous methylamines in the global atmosphere: impacts of oxidation and aerosol uptake. Atmos. Chem. Phys. 14, 12455–12464 (2014).
34. Norman, M. Distribution of marine boundary layer ammonia over the Atlantic and Indian Oceans during the Aerosols99 cruise. J. Geophys. Res. 110, D16302 (2005).
35. Rong, H. et al. Nucleation mechanisms of iodic acid in clean and polluted coastal regions. Chemosphere 253, 126743 (2020).
36. NASA POWER. Data access viewer. https://power.larc.nasa.gov/data-access-viewer/ (2022).
37. Khanniche, S., Louis, F., Cantrel, L. & Černušák, I. A theoretical study of the microhydration of iodic acid (HOIO2). Comput. Theor. Chem. 1094, 98–107 (2016).
38. Paasonen, P. et al. On the formation of sulphuric acid – amine clusters in varying atmospheric conditions and its influence on atmospheric new particle formation. Atmos. Chem. Phys. 12, 9113–9133 (2012).
39. Francl, M. M. et al. Self-consistent molecular orbital methods. XXIII. A polarization-type basis set for second-row elements. J. Chem. Phys. 77, 3654–3665 (1982).

40. Peterson, K. A., Figgen, D., Goll, E., Stoll, H. & Dolg, M. Systematically convergent basis sets with relativistic pseudopotentials. II. Small-core pseudopotentials and correlation consistent basis sets for the post- d group 16–18 elements. *J. Chem. Phys.* **119**, 11113–11123 (2003).

41. Xia, D. et al. Formation mechanisms of iodine–ammonia clusters in polluted coastal areas unveiled by thermodynamics and kinetic simulations. *Environ. Sci. Technol.* **54**, 9235–9242 (2020).

42. Frisch, M. J. et al. Gaussian 09 revision A.1. (2009).

43. Hattig, C. & Weigend, F. CC2 excitation energy calculations on large molecules using the resolution of the identity approximation. *J. Chem. Phys.* **113**, 5154–5161 (2000).

44. Kendall, R. A., Dunning, T. H. & Harrison, R. J. Electron affinities of the first-row atoms revisited. Systematic basis sets and wave functions. *J. Chem. Phys.* **96**, 6796–6806 (1992).

45. Pritchard, B. P., Altarawy, D., Didier, B., Gibson, T. D. & Windus, T. L. New basis set exchange: an open, up-to-date resource for the molecular sciences community. *J. Chem. Inf. Model.* **59**, 4814–4820 (2019).

46. Ahlrichs, R., Bär, M., Häser, M., Horn, H. & Kölmel, C. Electronic structure calculations on workstation computers: the program system turbomole. *Chem. Phys. Lett.* **162**, 165–169 (1989).

47. Kürten, A. et al. New particle formation in the sulfuric acid–dimethylamine–water system: reevaluation of CLOUD chamber measurements and comparison to an aerosol nucleation and growth model. *Atmos. Chem. Phys.* **18**, 845–863 (2018).

48. Carlsson, P. T. M. et al. Neutral sulfuric acid–water clustering rates: bridging the gap between molecular simulation and experiment. *J. Phys. Chem. Lett.* **11**, 4239–4244 (2020).

49. Li, H. et al. Influence of atmospheric conditions on sulfuric acid-dimethylamine-ammonia-based new particle formation. *Chemosphere* **245**, 125554 (2020).

50. Lu, T. & Chen, Q. Shermo: a general code for calculating molecular thermochemistry properties. *Comput. Theor. Chem.* **1200**, 113249 (2021).

51. Lu, T. & Chen, F. Multiwfn: a multifunctional wavefunction analyzer. *J. Comput. Chem.* **33**, 580–592 (2012).

52. Johnson, E. R. et al. Revealing noncovalent interactions. *J. Am. Chem. Soc.* **132**, 6498–6506 (2010).

53. Becke, A. *The Quantum Theory of Atoms in Molecules: From Solid State to DNA and Drug Design* (Wiley, 2007).

54. Elm, J. et al. Formation of atmospheric molecular clusters consisting of sulfuric acid and $C_8H_{12}O_6$ tricarboxylic acid. *Phys. Chem. Chem. Phys.* **19**, 4877–4886 (2017).

AUTHOR CONTRIBUTIONS

X.Z. contributed to conceiving the idea, analyzing results, editing, and revision. A.N. contributed to performing DFT and ACDC calculations, analyzing results and interpreting data, and writing the original draft. L.L., S.Z., L.D., and M.G. contributed to editing and revision. F.Y. contributed to performing GEOS-Chem simulations and editing.

COMPETING INTERESTS

The authors declare no competing interests.

ADDITIONAL INFORMATION

Supplementary information The online version contains supplementary material available at https://doi.org/10.1038/s41612-022-00316-9.

Correspondence and requests for materials should be addressed to Xiuhui Zhang.

Reprints and permission information is available at http://www.nature.com/reprints

Publisher's note Springer Nature remains neutral with regard to jurisdictional claims in published maps and institutional affiliations.